

Article

# $\beta$ -Cyclodextrin-Silica Hybrid: A Spatially Controllable Anchoring Strategy for Cu(II)/Cu(I) Complex Immobilization

Federica Calsolaro <sup>1</sup>, Katia Martina <sup>1,\*</sup>, Elisa Borfecchia <sup>2</sup>, Fernando Chávez-Rivas <sup>2,3</sup>, Giancarlo Cravotto <sup>1</sup> and Gloria Berlier <sup>2,\*</sup>

<sup>1</sup> Dipartimento di Scienza e Tecnologia del Farmaco, University of Turin, Via Pietro Giuria 9, 10125 Turin, Italy; federica.calsolaro@unito.it (F.C.); giancarlo.cravotto@unito.it (G.C.)

<sup>2</sup> Dipartimento di Chimica, University of Turin, Via Pietro Giuria 7, 10125 Turin, Italy; elisa.borfecchia@unito.it (E.B.); fchavez@esfm.ipn.mx (F.C.-R.)

<sup>3</sup> Departamento de Física, UPALM, Instituto Politécnico Nacional, ESFM, Zacatenco, Ciudad de México 07738, Mexico

\* Correspondence: katia.martina@unito.it (K.M.); gloria.berlier@unito.it (G.B.); Tel.: +39-011-6707168 (K.M.); +39-011-670-7856 (G.B.)

Received: 26 August 2020; Accepted: 23 September 2020; Published: 27 September 2020



**Abstract:** The development of new strategies for spatially controllable immobilization has encouraged the preparation of novel catalysts based on the organic-inorganic hybrid concept. In the present paper, a Cu-based multi-structured silica catalyst has been prepared and fully characterized. The inclusion of Cu(II) in  $\beta$ -cyclodextrins has been exploited with the double aim to stabilize the metal and to act as a source of Cu(I) catalytic sites. Multi-technique characterization by infrared, UV-visible, electron microscopy and X-ray absorption spectroscopies of the fresh and exhaust catalysts provided information on the local structure, redox properties and stability of the investigated hybrid systems. The catalytic system showed that copper nanospecies were dispersed on the support and hardly affected by the catalytic tests, confirming the stabilizing effect of  $\beta$ -CD, and likely of the N1-(3-Trimethoxysilylpropyl) diethylenetriamine spacer, as deduced by X-ray absorption spectroscopy analysis. Overall, we demonstrate a feasible approach to efficiently anchor Cu(II) species and to obtain a reusable single-site hybrid catalyst well suited for Cu(I)-catalyzed alkyne-azide cycloaddition.

**Keywords:** copper-catalysis; silica;  $\beta$ -cyclodextrin; organic-inorganic hybrid material; green chemistry; diffuse reflectance UV-visible; X-ray absorption spectroscopy; infrared spectroscopy

## 1. Introduction

The demand for functional materials, that consist of both inorganic and organic components, is due to their potential use as platforms for different applications [1]. The modification of the composition on the molecular scale of hybrid materials makes them tuneable for the design of smart materials [2,3], that can be used in catalysis [4], biochemistry [5], photochemistry [6,7] and optoelectronics [8,9]. In order to prepare organic-inorganic hybrid systems, an efficient surface modification of the inorganic part is required [10] and different synthetic strategies can be followed. The most used grafting procedure is represented by physical absorption (van der Waals forces, electrostatic and hydrogen bond interactions). However, several problems, such as inhomogeneous dispersions of the organic layer, can be observed when weak physical interactions are present between the organic and the inorganic portions [11]. A selective covalent grafting between the organic and the inorganic components represents a valuable alternative [11,12], preserving the structure, morphology and porosity of the supporting material [13].

Covalent bonds generate atomic scale connections with a good control of functional groups density on the material surface [14].

Most explored inorganic supports are mesoporous materials [15–18], polymers [19,20], nanostructured supports [21,22], metal organic frameworks (MOF) [23], etc. [24]. Surface exposed nucleophilic or electrophilic functions, vacant coordination sites and unsaturated functional groups can be used as active sites for specific derivatizations [13,25]. According to the type of derivatizing agent, the inorganic core can be grafted with three different types of molecules: small organic molecules [26], polymeric layer [27] and oligomeric molecules [28].

Hybrid nanostructures for catalytic applications have been studied and synthesized since the 1990s and still represent a big challenge for the scientific community, merging the heterogeneous and homogeneous worlds [29]. Solid supported catalysts show some advantages with respect to their homogeneous counterparts, but also some disadvantages. Their insolubility allows the product recovery, but the active catalytic species can be leached with the decrease in activity upon recycling. On the other hand, chemical modification by ligand grafting on the surface can enhance and tune the catalytic activity of supported metal sites [30]. The key role of the ligand is well recognized since it can impose stereo electronic effects, modify the electronic structure of metal, and interfere with the metal/solvent boundaries [31]. An important synthetic strategy entails the insertion of an organic flexible spacer between the ligand and the inorganic support to increase the accessibility and the stability of metallic sites [32]. Multidentate N-donor ligands have been largely employed in the preparation of organic-inorganic hybrid catalysts due to their versatile coordination modes [33,34]. So far, the vast majority of these approaches relied on the use of “innocent” ligands (i.e., not involved in any redox-activity); therefore, the metal oxidation state is assigned without complication [35]. Literature research in organic-inorganic hybrid systems for catalysis indeed revealed that in general not-innocent ligands have not received much attention to date [36].

$\beta$ -Cyclodextrins ( $\beta$ -CDs) can be used as carriers and stabilizers when grafted on the external surface of inorganic supports [37]. Thanks to their ability to host and stabilize metal ions and salts [38–40], CDs are widely exploited for the preparation of heterogeneous catalysts [21,41–44]. They can be employed for the spatial control of the catalyst as a result of a chemical confinement of the metallorganic species [45].  $\beta$ -CDs can be directly bound on the external surface of the inorganic support [46], or they can be bound to the inorganic surface with the interposition of organic spacers [32,47,48]. Interestingly, CDs have been efficiently employed for coordinating Cu(II) in a sandwich-type coordinative inclusion complex [49] and the Cu(II)-CD complex has been already employed to perform click azide-alkyne cycloadditions [50], C-C coupling of aryl boronic acids [51] and synthesis of oxazolidinones [52]. Interestingly, the click azide-alkyne cycloaddition is known to be catalysed by Cu(I), which should be produced in situ from the CD-Cu(II) complexes [53,54].

Herein, on the basis of our previous experience [54], we compare different covalently grafted silica- $\beta$ -CD hybrid catalysts. The work is aimed to investigate the influence of different flexible amino-bearing spacers on the catalytic activity and efficiency of silica-CD-Cu(II) derivatives in click azide-alkyne cycloaddition. Complementary characterization techniques (infrared, X-ray absorption spectroscopy, TEM, UV-Vis in diffuse reflectance) were used to obtain detailed information on the surface functionalization of the silica support, on the oxidation state, local environment and aggregation of the encapsulated/anchored Cu species, focusing on the stability and recyclability of the prepared materials.

## 2. Results and Discussion

### 2.1. Preparation and Characterization of Silica- $\beta$ -CD Derivatives

With the aim to study the influence of amino-bearing ligands in organic-inorganic silica-based Cu(II) catalysts, six different systems were synthesised and compared (Figure 1).  $\beta$ -CD was directly bound to the silica (Si-NH-CD), it was grafted through a diethylenetriamine spacer (Si-DETA-CD) or it was grafted through different monoamino, diamino and triamino alkoxy silyl spacers to obtain

Si-MonoAm-CD, Si-DiAm-CD and Si-TriAm-CD, respectively. The strategy focused on the use of flexible amino spacers and for sake of comparison the amino-CD was directly bound on the silica surface, and an amino alcohol spacer (Si-Gly-CD) was also studied.

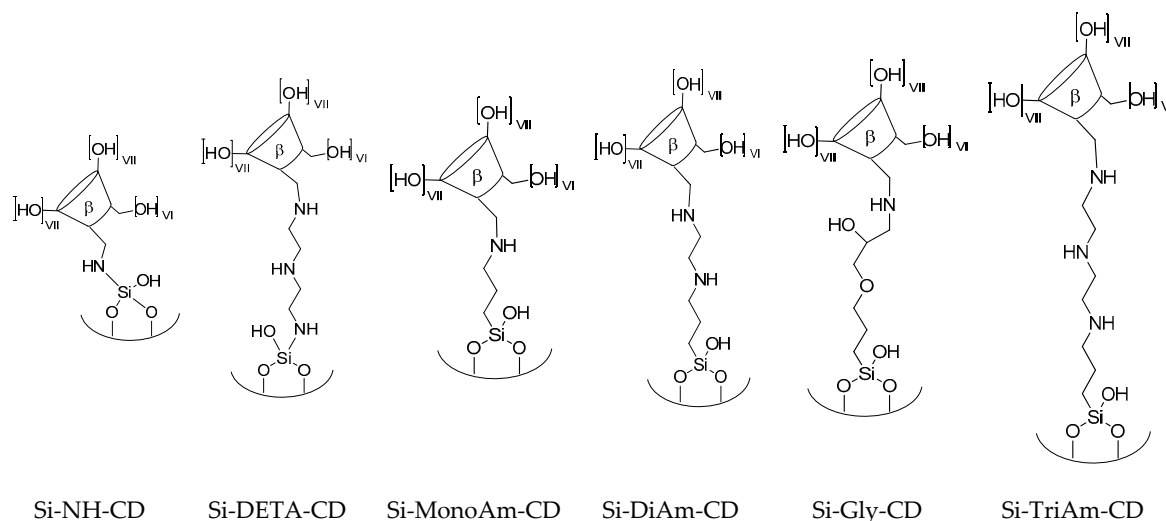
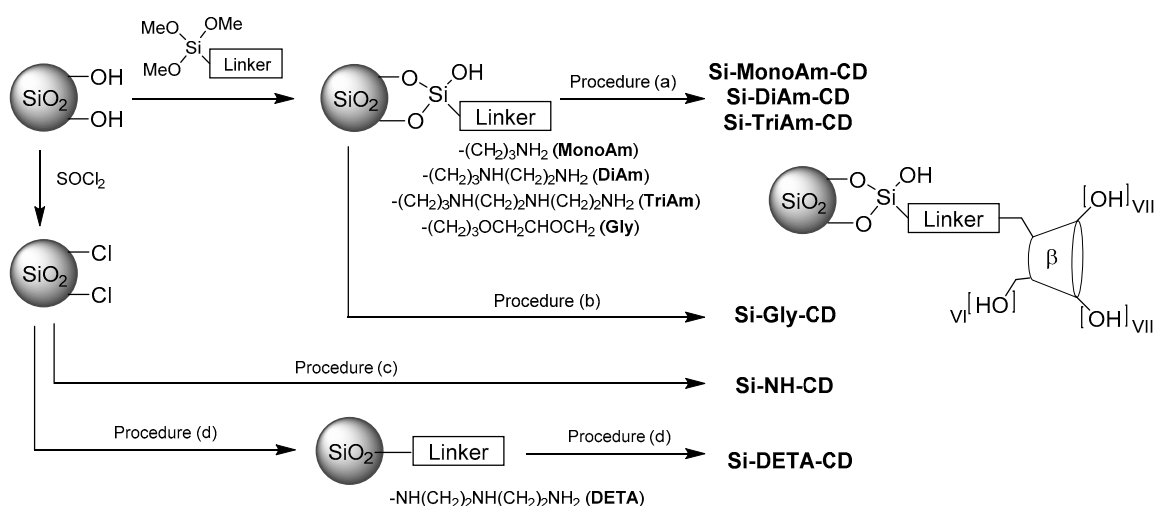


**Figure 1.** Structures of prepared silica- $\beta$ -CD derivatives.

On the basis of our experience [54], as depicted in Scheme 1, the external surface of the inorganic material (precipitated silica SIPERNAT 320—Evonik) was grafted with a thin organic layer thanks to the beneficial effects of ultrasound (US) irradiation that maximize the grafting loading. 6<sup>I</sup>-tosyl  $\beta$ -CD was the key intermediate for obtaining  $\beta$ -CD grafted silica (Scheme 1, procedure a), through nucleophilic substitution of the amino group. Efficient grafting of  $\beta$ -CD was achieved in 4 h at 100 °C in a combined microwave (MW)–US reactor. In the same way, 6<sup>I</sup> amino-6<sup>I</sup>-deoxy- $\beta$ -CD was reacted with Si-Gly to obtain Si-Gly-CD (Scheme 1, procedure b), or it was directly bound to silica, previously converted to silica chloride (Scheme 1, procedure c). When DETA spacer was used, silica was previously converted to silica chloride, using thionyl chloride, followed by nucleophilic substitution with DETA and 6<sup>I</sup>-tosyl  $\beta$ -CD (Scheme 1, procedure d).



**Scheme 1.** Synthetic scheme for the preparation of silica  $\beta$ -CD derivatives. Reaction conditions of procedure (a): amino grafted silica was reacted with 6<sup>I</sup>-tosyl  $\beta$ -CD in DMF; procedure (b): Si-Gly was reacted with 6<sup>I</sup> amino-6<sup>I</sup>-deoxy- $\beta$ -CD; procedure (c): silica was firstly functionalized with SOCl<sub>2</sub> and progressively grafted with 6<sup>I</sup> amino-6<sup>I</sup>-deoxy- $\beta$ -CD; procedure (d): silica was firstly functionalized with SOCl<sub>2</sub>, progressively grafted with diethylenetriamine and 6<sup>I</sup>-tosyl  $\beta$ -CD.

The loading and the identity of the synthesised silica derivatives were confirmed by thermogravimetric analysis (TGA) and infrared spectroscopy. From the percentage weight loss in the TGA curve, the amount of silyl amino portion and  $\beta$ -CD on silica surface was estimated. To exclude loss of adsorbed solvent molecules, the selected temperature range was from 150 °C to 800 °C. Furthermore, the loss of UV absorbance of phenolphthalein (Php) when included in the  $\beta$ -CD cavity was exploited to quantify grafted  $\beta$ -CD with unchanged inclusive properties [55]. UV spectra of not included Php in 10.5 water solution after treatment with a weighted amount of  $\beta$ -CD-silica derivatives were recorded at 553 nm and the amount of grafted  $\beta$ -CD was measured via interpolation from the standard curve. As shown in Figure 2, TGA analyses of Si-Gly, Si-MonoAm, Si-DiAm and Si-TriAm showed a high degree of derivatisation, from 6 to 12 *w/w* %, as reported in Table 1 (entries 2–5). The first derivative peak temperature was detected at 406 °C in Si-TriAm, 486 °C in Si-Gly, 495 °C in Si-MonoAm and 314 °C in Si-DiAm, and profiles were consistent in all samples. When Si-MonoAm-CD, Si-DiAm-CD and Si-TriAm-CD were analysed, 3.82% *w/w*, 7.66% *w/w* and 7.7% *w/w* of  $\beta$ -CD derivatisation were observed by TGA (34; 67, 68  $\mu\text{mol/g}$ , respectively). The Php titration showed that from 1.28% to 3.60% *w/w* of CD is available for making inclusion complexes (11 to 32  $\mu\text{mol/g}$ ). (Table 1, entry 7–9). In Si-Gly-CD, 6.08% *w/w* (54  $\mu\text{mol/g}$ ) of derivatisation was afforded by TGA and 1.04% *w/w* (9  $\mu\text{mol/g}$ ) was registered by Php titration (Table 1, entry 10). As shown in Figure 2, the TGA profile of Si-MonoAm-CD indicates that two degradation peaks, approximately at 360 °C and 519 °C, are visible, as well as in Si-Gly-CD (347 °C and 572 °C). When CD is grafted to Si-DiAm, two degradation steps are visible and are at 298 °C and 413 °C, as well as in Si-TriAm (339 °C and 584 °C). TGA profile of Si-DETA derivative shows a lower thermal stability if compared to the other chemically modified silica (Si-Gly, Si-MonoAm, Si-DiAm and Si-TriAm). In agreement with previous results, Si-DETA showed a certain instability when reacted with  $\beta$ -CD (see FT-IR description in ref 53) and herein we can confirm by thermogravimetric analysis that the use of condensation reaction between silanol groups of the silica surface and alkoxy silane generates more stable amine-bearing silica materials (see Supplementary Materials). To avoid the risk of chemical degradation of the solid supported catalyst, Si-DETA was discarded.

Si-Gly-CD, Si-MonoAm-CD, Si-DiAm-CD and Si-TriAm-CD (Table 1, entries 7–10) were loaded with Cu(II).  $\text{CuSO}_4$  was chosen as a Cu(II) source and it was loaded on silica-support- $\beta$  CD derivative in alkaline solution, obtaining blue colored catalyst.

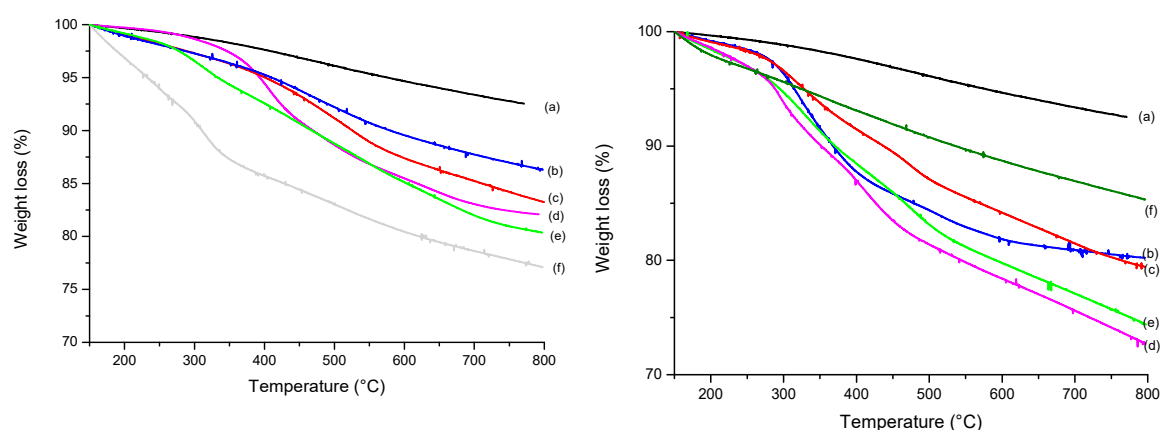


**Figure 2.** TGA profiles of organic inorganic silica derivatives. **On the left:** (a) silica, (b) Si-Gly, (c) Si-MonoAm, (d) Si-TriAm, (e) Si-DiAm, (f) Si-DETA (Table 1, entry 1–5). **On the right:** (a) silica, (b) Si-Gly-CD, (c) Si-MonoAm-CD, (d) Si-TriAm-CD, (e) Si-DiAm-CD, (f) Si-NHCD (Table 1, entry 6–10).

**Table 1.** Synthesis of grafted silica.

Entry	Product	Linker	Loading [w/w%]	Loading [μmol/g]
1	Si-DETA	-NH(CH <sub>2</sub> ) <sub>2</sub> NH(CH <sub>2</sub> ) <sub>2</sub> NH <sub>2</sub>	15.3 <sup>(a)</sup>	1.5 × 10 <sup>3</sup> <sup>(a)</sup>
2	Si-MonoAm	-(CH <sub>2</sub> ) <sub>3</sub> NH <sub>2</sub>	9.19 <sup>(a)</sup>	513 <sup>(a)</sup>
3	Si-DiAm	-(CH <sub>2</sub> ) <sub>3</sub> NH(CH <sub>2</sub> ) <sub>2</sub> NH <sub>2</sub>	12.1 <sup>(a)</sup>	543 <sup>(a)</sup>
4	Si-TriAm	-(CH <sub>2</sub> ) <sub>3</sub> NH(CH <sub>2</sub> ) <sub>2</sub> NH(CH <sub>2</sub> ) <sub>2</sub> NH <sub>2</sub>	10.36 <sup>(a)</sup>	390 <sup>(a)</sup>
5	Si-Gly	-(CH <sub>2</sub> ) <sub>3</sub> OCH <sub>2</sub> CHOCH <sub>2</sub>	6.13 <sup>(a)</sup>	259 <sup>(a)</sup>
6	Si-NH-CD	-NH-βCD	7.12 <sup>(b)</sup> -0.68 <sup>(c)</sup>	62 <sup>(b)</sup> -6 <sup>(c)</sup>
7	Si-MonoAm-CD	-(CH <sub>2</sub> ) <sub>3</sub> NH-βCD	3.82 <sup>(b)</sup> -1.28 <sup>(c)</sup>	34 <sup>(b)</sup> -11.3 <sup>(c)</sup>
8	Si-DiAm-CD	-(CH <sub>2</sub> ) <sub>3</sub> NH(CH <sub>2</sub> ) <sub>2</sub> NH-βCD	7.66 <sup>(b)</sup> -2.09 <sup>(c)</sup>	67 <sup>(b)</sup> -18.4 <sup>(c)</sup>
9	Si-TriAm-CD	-(CH <sub>2</sub> ) <sub>3</sub> NH(CH <sub>2</sub> ) <sub>2</sub> NH(CH <sub>2</sub> ) <sub>2</sub> NH-βCD	7.7 <sup>(b)</sup> -3.60 <sup>(c)</sup>	68 <sup>(b)</sup> -32 <sup>(c)</sup>
10	Si-Gly-CD	-(CH <sub>2</sub> ) <sub>3</sub> OCH <sub>2</sub> CHOHCH <sub>2</sub> -βCD	6.08 <sup>(b)</sup> -1.04 <sup>(c)</sup>	54 <sup>(b)</sup> -9.2 <sup>(c)</sup>

Preparation of Si-Gly, Si-MonoAm, Si-DiAm, Si-TriAm: silica powder (0.100 g), toluene (1 mL), mono and poly amino alkoxy silane derivatives (0.040 mL), US (80 kHz, 2 h). Preparation of Si-MonoAm-CD, Si-DiAm-CD, Si-TriAm-CD: Si-MonoAm, Si-DiAm or Si-TriAm (1 g), DMF (15 mL), 6<sup>1</sup>-tosyl-β-CD (1 g), MW/US (100 °C, 4 h). Preparation of Si-Gly-CD: Si-Gly (1 g), DMF (15 mL), 6<sup>1</sup> amino-6<sup>1</sup>-deoxy-β-CD (1 g), MW/US (100 °C, 4 h) <sup>(a)</sup> measured by TGA; <sup>(b)</sup> β-CD grafting measured by TGA; <sup>(c)</sup> β-CD grafting measured by PhP titration.

The prepared materials were characterized by infrared and diffuse reflectance (DR) UV-Vis spectroscopies, to assess the molecular structure of the final products (Figure 3). The infrared spectra of the four samples show the fingerprint modes of CD between 1500 and 1250 cm<sup>-1</sup> (δCH and δOH bending modes) with variable intensity and shape (Figure 3, left hand panel). The intense peak at 1664 cm<sup>-1</sup>, labeled with a star in the Figure, can be ascribed to the presence of residual DMF solvent. The effective bonding of the functional groups is furthermore proven by the intense CH/CH<sub>2</sub> stretching modes (νCH/CH<sub>2</sub>) at 2928 and 2856 cm<sup>-1</sup>. These are superimposed to the broad absorption related to hydrogen bonded -OH and -NH groups, including OH groups from the CD rings and Si-OH groups from the silica surface [54,56]. Both Si-DiAm-CD-Cu and Si-TriAm-CD show a component around 1596 cm<sup>-1</sup>, typical of the bending mode of primary amines (δNH<sub>2</sub>), which would indicate an incomplete reaction of the amino groups with CDs.

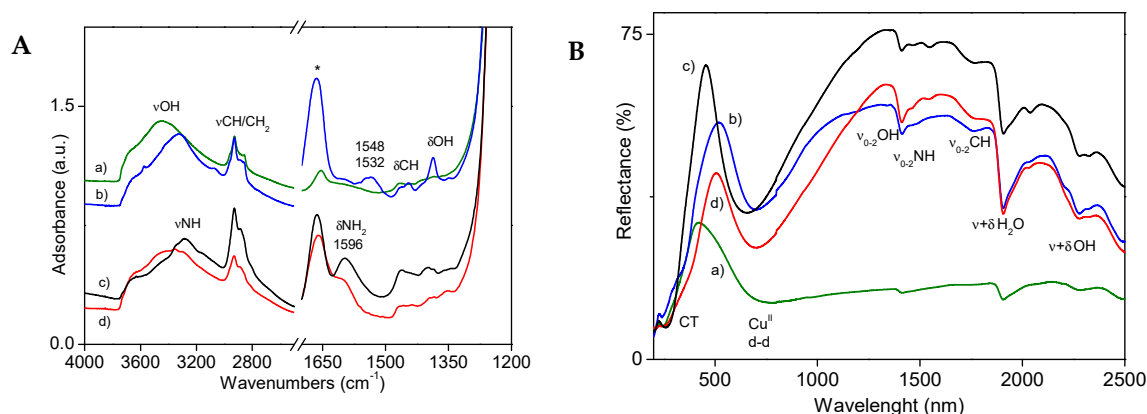


**Figure 3.** Infrared (A) and diffuse reflectance UV-Vis (B) spectra of (a) Si-Gly-CD-Cu; (b) Si-MonoAm-CD-Cu; (c) Si-DiAm-CD-Cu; (d) Si-TriAm-CD-Cu. Before infrared measurements samples were outgassed at 80 °C to remove adsorbed water and impurities. The peak labeled with \* can be related to DMF residual solvent.

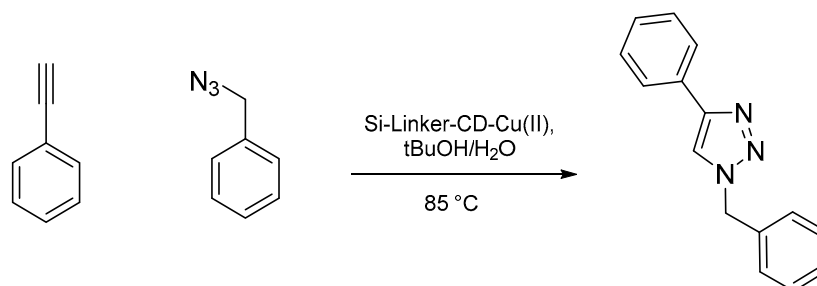
Weak overtone modes of the νCH and νNH vibrations (ν<sub>0-2</sub>) can be also appreciated in the low energy region of the corresponding DR UV-Vis spectra (Figure 3, right), which are reported in reflectance mode (negative peaks), to avoid artefacts related to the Kubelka–Munk conversion. Apart from sample Si-Gly-CD-Cu, which shows relatively weak peaks in the whole spectral range, the three samples functionalized with amino groups very clearly show the typical d-d transition of Cu(II) ions around 700 nm, though with some difference in the band width and position. In agreement with

previous reports, this can be used as a fingerprint of Cu(II) ions stabilized in the cavity. These could be hexacoordinated, as a result of coordination by H<sub>2</sub>O, OH/O<sup>-</sup> CD groups or extra-ligands [38] or have lower coordination, in square planar geometry [57].

## 2.2. Catalytic Activity of Organic-Inorganic Silica-Supported $\beta$ -CD-Cu(II)

Based on the catalytic activity of silica-supported  $\beta$ -CD-Cu(II) previously studied [54], as-prepared systems were tested in alkyne-azide cycloaddition (CuAAC). The interaction between  $\beta$ -CD and Cu ions could implicate the reduction of Cu(II) to Cu(I), as proved afterwards by X-ray absorption spectroscopy (XAS, see Section 2.3). CuAAC were conducted in the absence of reducing agents and the copper amount was assumed to be the same as measured by inductively coupled plasma (ICP) on the Si-DiAm-CD-Cu (15.5 mg/g). The reaction between benzyl azide and phenyl acetylene was chosen as model reaction (Scheme 2). The most active silica catalyst was proven to be Si-TriAm-CD-Cu (Table 2, entries 6–8). It reacts efficiently not only with the model reaction but also with the more demanding synthesis of dimer in the presence of diazide or dialkynyl derivatives, as shown in Table 3 (entries 5–6). As depicted in Table 2, we can assume that the amino-bearing spacer can stabilize Cu(II) species and it allows Cu ions to be more accessible.

To demonstrate the reaction applicability on different types of reagents, the most active Si-TriAm-CD-Cu was tested on a small set of alkyne and azide derivatives and full conversions were observed with 4 or 8.7 mol.% of catalyst. The products were isolated without purification and interestingly, the catalyst was observed to be suitable for dimer synthesis in high yield (Table 3, entries 5–6).



**Scheme 2.** Model reaction for CuAAC of Si-Linker-CD-Cu.

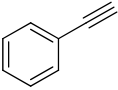
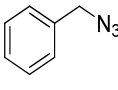
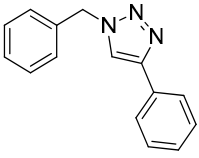
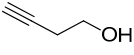
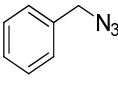
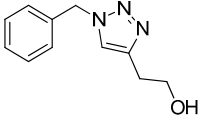
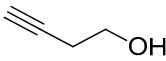
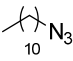
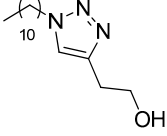
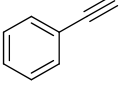
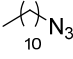
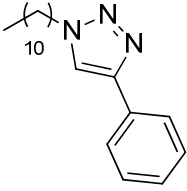
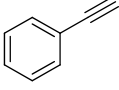
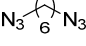
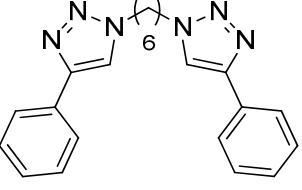
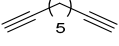
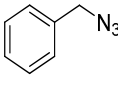
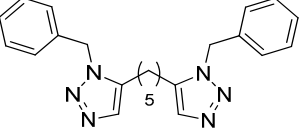
**Table 2.** Panel test of CuAAC reaction.

Entry	Catalyst	Cu mol. %	Yield [%] <sup>(a)</sup>
1	Si-NHCD-Cu	4	5 <sup>(b)</sup>
2	Si-DiAm-CD-Cu	4	>99 <sup>(b)</sup>
3	Si-DiAm-CD-Cu	2	65 <sup>(b)</sup>
4	Si-Gly-CD-Cu	4	45
5	Si-MonoAm-CD-Cu	4	4
6	Si-TriAm-CD-Cu	4	>99
7	Si-TriAm-CD-Cu	2	>99
8	Si-TriAm-CD-Cu	1	85

Reaction conditions: benzyl azide (0.0676 mmol, 1 eq), phenylacetylene (1 eq), H<sub>2</sub>O:tBuOH (1:1; 500  $\mu$ L), 85 °C, 1 h.

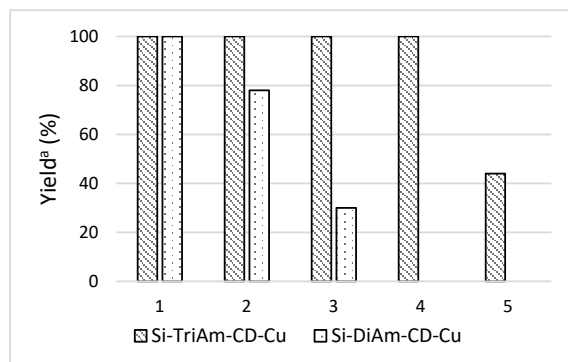
<sup>(a)</sup> Yields determined by gas chromatography–mass spectrometry (GC-MS); <sup>(b)</sup> Tests conducted and reported in our previous work [54].

Table 3. Cu-supported catalysed CuAAC.

Entry	Alkyne	Azide	Product	Yield [%] <sup>(a)</sup>
1				99
2				99 <sup>(b)</sup>
3				99 <sup>(b)</sup>
4				99 <sup>(b)</sup>
5				99 <sup>(c)</sup>
6				99 <sup>(d)</sup>

<sup>(a)</sup> Yields determined by GC-MS. Reaction conditions: azide (0.0676 mmol, 1 eq), terminal alkyne (1 eq), H<sub>2</sub>O (250  $\mu$ L), *t*BuOH (250  $\mu$ L), catalyst (4 mol.%), 85 °C, 1 h; <sup>(b)</sup> catalyst (8.7 mol.%), reaction time 5 h; <sup>(c)</sup> terminal alkyne (2 eq), catalyst (8.7 mol.%), reaction time 5 h; <sup>(d)</sup> azide (2 eq), catalyst (8.7 mol.%), reaction time 5 h.

A study on the recoverability and recyclability of Si-DiAm-CD-Cu and Si-TriAm-CD-Cu catalysts was performed on a CuAAC model reaction. The following reaction conditions were used: reaction temperature of 85 °C; H<sub>2</sub>O/*t*BuOH ratio of 1:1; reaction time of 1 h; amount of catalyst 4 mol.%. The catalysts were recovered by filtering the reaction mixture and washing with water, methanol and chloroform. After drying, they were reused in the reaction. Figure 4 displays the performance of the reused catalysts. After four cycles, the reaction yield using Si-TriAm-CD-Cu was 44%. The recovery of the catalyst indicates its good structural stability and high reactive activity. If compared to Si-DiAm-CD-Cu catalyst, it shows higher stability. The reaction yield of Si-DiAm-CD-Cu was 78% in the second reuse, and 30% in the third cycle.



**Figure 4.** Recyclability of Si-TriAm-CD-Cu, compared to Si-DiAm-CD-Cu, in the CuAAC model reaction.

### 2.3. Characterization of Aged Si-TriAm-CD-Cu Catalyst

Sample Si-TriAm-CD-Cu was further characterized after the catalytic tests by infrared, DR UV-Vis and XAS spectroscopies. The infrared spectrum measured on the sample recovered after catalytic tests is indistinguishable from that of the as-prepared material, indicating the stability of the grafted groups (Figure 5, left panel). Some differences can instead be observed in the DR UV-Vis spectra (Figure 5, right panel), particularly in the intensity of the Cu(II) band. The comparison is not quantitative, since the exhaust sample (five time reused catalyst) was measured after dilution in Teflon, due to the small amount recovered from the catalytic tests. The reported spectrum is indeed roughly normalized with respect to the overtone/combination modes in the near infrared (NIR) region ( $\nu + \delta$  of H<sub>2</sub>O and OH). Notwithstanding these limitations, the results are in agreement with a decrease in the amount of Cu(II) in the catalyst, which can be tentatively related to a partial reduction to Cu(I), which is silent in the UV-Vis d-d region being a closed shell d<sup>10</sup> ion. This hypothesis was further investigated by XAS (see below).

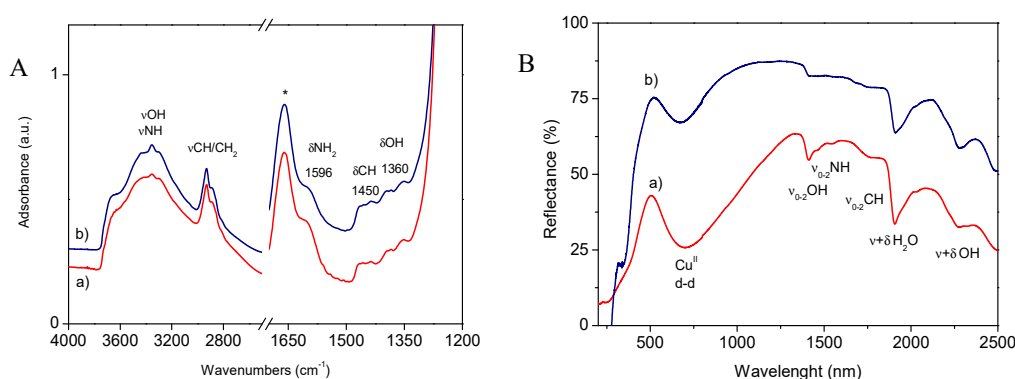
To obtain more insight on the oxidation state and local coordination environment of the Cu centers in Si-TriAm-CD-Cu, we characterized the as-prepared vs. exhaust catalyst by Cu K-edge XAS. The technique, combining element-selective response with simultaneous sensitivity to local electronic and structural properties of Cu-species [58,59], is complementary to the IR and UV-Vis results discussed before.

Figure 6 reports the obtained results for Si-TriAm-CD-Cu, in both the X-ray absorption near edge structure (XANES) and the extended X-ray absorption fine structure (EXAFS) regions (Figure 6a,b, respectively). The XAS spectra of the as-prepared and exhaust catalyst are compared to the ones obtained for selected model compounds, including Cu(II) and Cu(I) oxides. A Cu(II) complex with mixed N/O ligation is also considered, characterized as [Cu<sup>II</sup>(NH<sub>3</sub>)<sub>3</sub>(NO<sub>3</sub>)]<sup>+</sup> in a previous study [60], where Cu(II) is coordinated in a pseudo-square planar fashion to three N(NH<sub>3</sub>) and to one O(NO<sub>3</sub>) atom.

XAS reveals that as-prepared Si-TriAm-CD-Cu exclusively contains Cu(II) species, based on the absorption edge position, as well as on the presence of a characteristic rising-edge peak at ca. 8986 eV. Indeed, this XANES feature, observed for both Cu<sup>II</sup>O and [Cu<sup>II</sup>(NH<sub>3</sub>)<sub>3</sub>(NO<sub>3</sub>)]<sup>+</sup> model compounds is assigned to three/four-fold coordinated Cu<sup>II</sup> metal centers [59,61]. The XANES line shape observed



for Si-TriAm-CD-Cu in correspondence of the intense resonance at ca. 8995 eV (“white-line” peak region) resembles the one observed in the  $[\text{Cu}^{\text{II}}(\text{NH}_3)_3(\text{NO}_3)]^+$ , pointing to a possible mixed ligation to both O (e.g., from OH groups), and N atoms (most likely from the  $\text{N}^1$ -(3-Trimethoxysilylpropyl) diethylenetriamine spacer) of Cu-species in the as-prepared catalyst. EXAFS spectra also indicate for Si-TriAm-CD-Cu a ligand environment similar to the one in  $\text{Cu}^{\text{II}}(\text{NH}_3)_3(\text{NO}_3)^+$ , resulting in almost overlapped first-shell peaks. Notably, the first-shell intensity is, in these cases, intermediate between the one detected for  $\text{Cu}_2\text{O}$  (two O neighbors) and  $\text{Cu}^{\text{II}}\text{O}$  (four O neighbors in ideal square planar coordination). This observation is consistent with the presence in Si-TriAm-CD-Cu of four-fold-coordinated Cu(II) sites with both N- and O-containing ligands. Comparing the EXAFS of Si-TriAm-CD-Cu with the ones of bulk Cu-oxides at higher R-values, it clearly emerges that no trace of high-intensity Cu-Cu scattering contributions compatible with large oxidic or metallic aggregates is detected, while a well-defined second-shell peak is observed. This is consistent with the presence of highly dispersed Cu-species, in the form of monomers or very small clusters.



**Figure 5.** Infrared (A) and diffuse reflectance UV-Vis (B) spectra of (a) Si-TriAm-CD-Cu; (b) Si-TriAm-CD-Cu-exhaust. Before infrared measurements samples were outgassed at 80 °C to remove adsorbed water and impurities. Sample Si-TriAm-CD-Cu-exhaust was diluted in Teflon for Diffuse-Reflectance (DR) UV-Vis measurement. The corresponding curve was arbitrarily normalized to the intensity of the overtone/combination modes of the support ( $\times 2.5$ ). The peak labeled with \* can be related to DMF residual solvent.

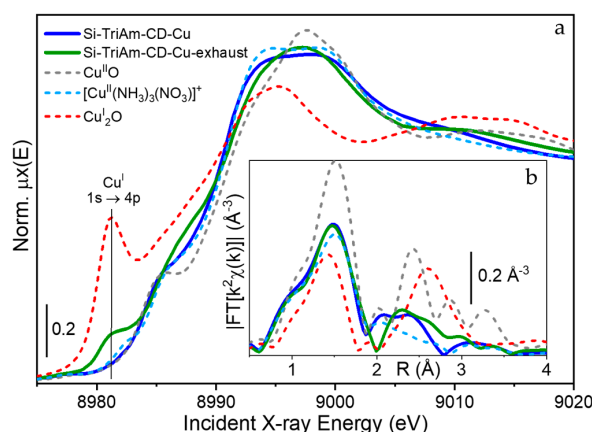


**Figure 6.** Cu K-edge (a) X-ray absorption near edge structure (XANES) and (b) extended X-ray absorption fine structure (EXAFS) spectra of Si-TriAm-CD-Cu and Si-TriAm-CD-Cu five times reused reported as thick solid lines. The spectra of the sample are compared to the ones of selected model compounds, namely  $\text{Cu}^{\text{II}}\text{O}$ ,  $\text{Cu}_2\text{O}$ , and  $[\text{Cu}^{\text{II}}(\text{NH}_3)_3(\text{NO}_3)]^+$ , reported as thin dashed lines.

In line with the UV-Vis results, XAS analysis of exhaust Si-TriAm-CD-Cu unambiguously indicates the formation of a small fraction of Cu(I). Indeed, we observe the appearance of an additional rising-edge peak at ca. 8982 eV, occurring at the same energy position as seen in  $\text{Cu}_2\text{O}$  and representing a fingerprint

of Cu(I) species [59,61,62]. On the other hand, the EXAFS signals of the two samples are very similar, apart from small differences in correspondence of the second shell peak around 2.5 Å, which are not compatible with the formation of large metal or oxidic aggregates (compare with grey and red dashed lines in Figure 6b). This indicates that, besides the change in the oxidation state of a fraction of the copper, the average local environment and agglomeration of the metal centers is not sensibly affected by catalysis. This is an important observation, confirming on one hand the stabilizing effect of the amino spacer and CD on the copper catalytic centers, and on the other hand the formation of catalytically active Cu(I) ions during the reaction.

The high dispersion of Cu on the silica functionalized material is further confirmed by Transmission Electron Microscopy (TEM). The sample is characterized by aggregates of silica nanoparticles with sizes of around 10–15 nm, which are not affected in size, morphology and aggregation by the catalytic tests (Figure 7a, referring to the two times reused catalyst). Higher magnification images of Si-TriAm-CD-Cu (as prepared and two times reused catalyst, Figure 7b,c, respectively) suggest the presence of very small (a few nanometers) Cu nanoparticles, which can be seen as dark spots in both materials. The particle size is too small to give electron diffraction, which would give more detailed information on their structure. No diffraction spots could be observed by selected area electron diffraction (SAED) on different portions of the samples. Putting together this piece of information with EXAFS data, which exclude the presence of a significant fraction ( $\geq 10\%$ ) of large aggregates, we can ascertain the high dispersion of the Cu species. Obviously, this is only a qualitative observation, and more specific measurement (such as  $N_2O$  chemisorption) would be necessary for a quantitative analysis of copper dispersion, which is outside the scope of this work.

ICP analysis was also performed on the freshly prepared and exhaust catalyst. The data demonstrated a copper quantity of 14.9 mg/g and 14.1 mg/g, respectively, showing 5% leaching. What is relevant, is that copper species ( $\beta$ -CD-Cu and Cu NPs) are highly dispersed on the support and hardly affected by the catalytic tests, confirming the stabilizing effect of  $\beta$ -CD, and likely of the  $N^1$ -(3-Trimethoxysilylpropyl) diethylenetriamine spacer, as suggested by XAS data.

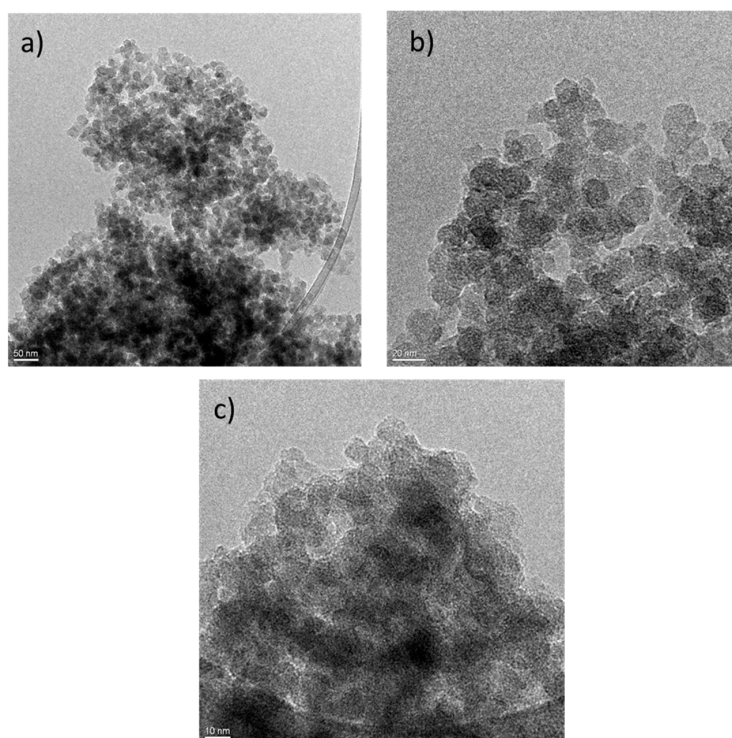


**Figure 7.** TEM images of Si-TriAm-CD-Cu-two times reused (a,b) Si-TriAm-CD-Cu (c).

### 3. Materials and Methods

#### 3.1. Materials

The US bath was supplied by Weber Ultrasonics AG (Karlsbad, Germany). The combined system MW/US was designed in our laboratory and a sonic horn (made of Pyrex<sup>®</sup>) was inserted inside a MW cavity (Milestone s.r.l., RotoShynth reactor). TGA were performed with a TGA 4000 (Perkin Elmer, Waltham, MA, USA); operating conditions: 10–20 mg of sample, rate 10 °C min<sup>-1</sup> from 50 °C to 800 °C, argon atmosphere. UV spectra were measured on a dual-beam spectrophotometer (Agilent Technologies Cary 60, G6860AA, Santa Clara, CA, USA) using a 1 cm path length cuvette. A GC Agilent 6890 (Agilent Technologies, Santa Clara, CA, USA), fitted with a mass detector Agilent Network 5973, was used for GC-MS analyses. A MALDI-TOF mass spectra (Bruker Ultraflex TOF mass spectrometer, Milan, Italy) was used to determine HRMS. The cations were determined with a Perkin Elmer Optima 7000 (Perkin Elmer, Waltham, MA, USA) inductively coupled plasma-optical emission spectrometer (ICP-OES). Jeol ECZ-R at 25 °C, 600 MHz and 75 MHz for <sup>1</sup>H and <sup>13</sup>C, respectively, was used to record NMR spectra.

#### 3.2. Catalyst Preparation

Si-NHCD, Si-DETA, Si-DETA-CD, Si-DiAm, Si-DiAm-CD were prepared following the reaction procedures reported in the literature [54].

##### 3.2.1. General Preparation of Alkoxy Silyl-Silica Derivatives (Si-Gly, Si-MonoAm, Si-TriAm)

Alkoxy silyl alkyl compound (0.040 mL) was dissolved in toluene (1 mL) and silica (0.100 g) was added. The mixture was sonicated 2 h in US bath (Power 200 W, Frequency 80 kHz). The product was filtered and washed with toluene and chloroform. Finally, it was dried under vacuum for 12 h (detailed information for alkoxy silyl-silica derivatives preparation are reported in Supplementary Materials).

##### 3.2.2. General Preparation of Silica-β-CD Hybrid Systems (Si-Gly-CD, Si-MonoAm-CD, Si-TriAm-CD)

First, 6<sup>l</sup>-derivatized-β-CD (1 g) was dissolved in DMF (15 mL). Then, alkoxy silyl-silica derivative (1 g) was added. The suspension was irradiated under MW and US combined irradiation at 100 °C for 4 h (MW power 20 W, US power 35 W). The product was filtered and washed with water, methanol and chloroform. Finally, it was dried under vacuum for 12 h (detailed information for silica-β-CD hybrid systems preparation are reported in Supplementary Materials).

##### 3.2.3. β-CD-Cu(II) Complexation

The silica-β-CD hybrid system (0.100 g) was dispersed in NaOH 0.5 M (0.675 mL). CuSO<sub>4</sub> 0.08 M (0.719 mL) was added dropwise, during US sonication. The suspension was immediately filtered and washed with water and methanol. Finally, the solid was dried under vacuum for 12 h.

#### 3.3. Click Chemistry Reaction

Azide (0.0676 mmol, 1 eq) and terminal alkyne (1 eq) were dissolved in H<sub>2</sub>O: *t*BuOH (0.500 μL, 1:1). Silica-β-CD-Cu(II) catalyst (2, 4 or 8.7 mol.%, see Table 2, entries 6–8; Table 3, entries 1–6) was added. The reaction was stirred at 85 °C, for 1 or 5 h. The mixture was filtered, washed with methanol and chloroform. The solvent was removed under vacuum. <sup>1</sup>H NMR and GC-MS were recorded to confirm triazole structure.

#### 3.4. Catalysts Characterization

Infrared spectra were recorded on a BRUKER FTIR-66 spectrophotometer with a resolution of 2 cm<sup>-1</sup>, using a MCT detector. Measurements were carried out using a home-made cell allowing in situ thermal treatment and room temperature measurement. Thin self-supporting pellets for transmission

measurements (around 10 mg/cm<sup>2</sup>) were prepared with a hydraulic press. Before the measurements, the samples were outgassed at 80 °C for 2 h in the same cell used for the measurements.

Diffuse reflectance UV-Vis-NIR spectra were recorded in the 200–2500 nm range at 1 nm resolution on a Cary 5000 UV-Vis-NIR spectrophotometer (Agilent) equipped with a diffuse reflectance attachment with an integrating sphere coated by BaSO<sub>4</sub>. Prior to each measurement, a baseline spectrum was collected by using Teflon as a reference. All samples were measured as such, expected for Si-TriAm-CD-Cu-exhaust, which was diluted in Teflon. Spectra are reported as relative reflectance (R%), defined as:

$$R\% = R_{\text{sample}}/R_{\text{reference}} \times 100$$

Cu K-edge XAS measurements were performed at the B18 beamline [63] of the Diamond Light Source (UK). XAS spectra were collected in transmission mode, by means of a fixed-exit double crystal water-cooled Si(111) monochromator and Pt-coated mirrors. We employed ionization chambers filled with different mixtures of He and Ar to measure the incident ( $I_0$ ) and transmitted ( $I_{1,2}$ ) X-ray intensities. A third ionization chamber ( $I_2$ ) was employed to simultaneously measure the XANES spectrum of a Cu metal foil, for the sake of energy calibration [58]. Si-TriAm-CD-Cu, in its as-prepared and exhaust state, was measured at RT in air, in the form of a self-supporting pellet, with optimized weight for transmission-mode XAS. The Cu<sup>II</sup>O and Cu<sup>I</sup><sub>2</sub>O model compounds were also measured in the form of self-supporting pellets, with optimized weights. Reported XAS spectra for [Cu<sup>II</sup>(NH<sub>3</sub>)<sub>3</sub>(NO<sub>3</sub>)]<sup>+</sup> are instead reproduced from ref. [60] to which the reader is referred for additional details on data acquisition and interpretation. The reported XAS spectra were collected on the B18 beamline in Quick-EXAFS mode, scanning the incident X-ray energy in the 8800–9783 eV range with a constant energy step of 0.3 eV. Data acquisition time was 3 min/scan. For each pelletized sample, we collected five consecutive Quick-EXAFS scans, subsequently averaged to enhance data quality after checking for signal reproducibility. We normalized to unity edge jump and aligned in energy all the XAS spectra using the Athena software from the Demeter package [64]. The Athena program was also employed to extract the  $\chi(k)$  EXAFS. Fourier-transform (FT) EXAFS spectra were calculated by transforming the  $k^2\chi(k)$  functions in the (2.4–12.0) Å<sup>-1</sup> range.

#### 4. Conclusions

In conclusion, the study evidenced the synergistic activity of silica,  $\beta$ -CD and of a polyamino spacer in obtaining spatially isolated and well-characterized active catalytic sites. The Cu(II)/ $\beta$ -CD complex was proven to act as an efficient source of Cu(I) species and multidentate N-donor ligands showed to activate and stabilize the catalytic species. A deep level of understanding was achieved by the combination of IR, DR UV-Vis, XAS and TEM analysis on the fresh and the exhaust catalyst. The applied characterization methods consistently demonstrated: (i) the successful incorporation and stability of the grafted functionalities; (ii) the exclusive presence of Cu(II) in the fresh catalysts, most likely occurring in a O/N mixed-ligand environment; (iii) the formation of few Cu(I) species in the catalyst after usage without substantial perturbations in the Cu local coordination environment and aggregation state. Complementary insights by TEM, in agreement with EXAFS results, confirmed that Cu remains highly dispersed on the support after the catalytic tests. The novel Cu-supported hybrid heterogeneous catalysts showed excellent performances in click reactions for the synthesis of small molecules and dimers.

**Supplementary Materials:** The following are available online at <http://www.mdpi.com/2073-4344/10/10/1118/s1>.

**Author Contributions:** Methodology and experimental design, K.M., G.B., G.C.; investigation, F.C., E.B., F.C.-R.; data curation, G.B., F.C., K.M.; catalyst analysis E.B., G.B., F.C., F.C.-R.; writing—original draft preparation, F.C., G.B., E.B. and K.M., writing—review and editing, G.B.; G.C. All authors have read and agreed to the published version of the manuscript.

**Funding:** This research received no external funding.

**Acknowledgments:** The authors acknowledge the University of Turin for the financial support (Ricerca Locale 2018). We acknowledge Diamond Light Source for time on Beamline B18 under Proposal SP21713-1 and D. Gianolio for support during the XAS measurements on B18.

**Conflicts of Interest:** The authors declare no conflict of interest.

## References

1. Chujo, Y. Organic-Inorganic hybrid materials. *Curr. Opin. Solid State Mater. Sci.* **1996**, *1*, 806–811. [[CrossRef](#)]
2. Férey, G. Hybrid porous solids: Past, present, future. *Chem. Soc. Rev.* **2008**, *37*, 191–214. [[CrossRef](#)] [[PubMed](#)]
3. Wen, J.; Wilkes, G.L. Organic/Inorganic Hybrid Network Materials by the Sol-Gel Approach. *Chem. Mater.* **1996**, *8*, 1667–1681. [[CrossRef](#)]
4. Mohammadi Ziarani, G.; Badiei, A.; Hajiabbas Tabar Amiri, P.; Lashgari, N. A Green Multicomponent One-pot Synthesis of 9, 10-Diaryl-7H-benzo [d,e] imidazo [2,1-a] isoquinolin-7-one Derivatives using Nanoporous Base Silica (SBA-Pr-NH<sub>2</sub>) as Catalyst. *J. Nanostruct.* **2019**, *9*, 1–7. [[CrossRef](#)]
5. Suganya, K.S.U.; Govindaraju, K.; Vani, C.V.; Premanathan, M.; Kumar, V.K.G. In vitro biological evaluation of anti-diabetic activity of organic-inorganic hybrid gold nanoparticles. *IET Nanobiotechnol.* **2019**, *13*, 226–229. [[CrossRef](#)] [[PubMed](#)]
6. Cariati, E.; Lucenti, E.; Botta, C.; Giovanella, U.; Marinotto, D.; Righetto, S. Cu(I) hybrid inorganic–organic materials with intriguing stimuli responsive and optoelectronic properties. *Coord. Chem. Rev.* **2016**, *306*, 566–614. [[CrossRef](#)]
7. Karthik, P.; Vinoth, R.; Selvam, P.; Balaraman, E.; Navaneethan, M.; Hayakawa, Y.; Neppolian, B. A visible-light active catechol–metal oxide carbonaceous polymeric material for enhanced photocatalytic activity. *J. Mater. Chem. A* **2017**, *5*, 384–396. [[CrossRef](#)]
8. Xiao, Z.; Kerner, R.A.; Zhao, L.; Tran, N.L.; Lee, K.M.; Koh, T.-W.; Scholes, G.D.; Rand, B.P. Efficient perovskite light-emitting diodes featuring nanometre-sized crystallites. *Nat. Photonics* **2017**, *11*, 108. [[CrossRef](#)]
9. Di Tommaso, S.; Giannici, F.; Mossuto Marculescu, A.; Chiara, A.; Tealdi, C.; Martorana, A.; Labat, F.; Adamo, C. Theoretical insights into inorganic-organic intercalation products of the layered perovskite HLaNb<sub>2</sub>O<sub>7</sub>: Perspectives for hybrid proton conductors. *Phys. Chem. Chem. Phys.* **2019**, *21*, 16647–16657. [[CrossRef](#)]
10. Dolbecq, A.; Dumas, E.; Mayer, C.R.; Mialane, P. Hybrid Organic–Inorganic Polyoxometalate Compounds: From Structural Diversity to Applications. *Chem. Rev.* **2010**, *110*, 6009–6048. [[CrossRef](#)]
11. Lei, B.; Li, B.; Zhang, H.; Zhang, L.; Li, W. Synthesis, Characterization, and Oxygen Sensing Properties of Functionalized Mesoporous SBA-15 and MCM-41 with a Covalently Linked Ruthenium(II) Complex. *J. Phys. Chem. C* **2007**, *111*, 11291–11301. [[CrossRef](#)]
12. Franville, A.-C.; Zambon, D.; Mahiou, R.; Troin, Y. Luminescence Behavior of Sol–Gel-Derived Hybrid Materials Resulting from Covalent Grafting of a Chromophore Unit to Different Organically Modified Alkoxysilanes. *Chem. Mater.* **2000**, *12*, 428–435. [[CrossRef](#)]
13. Benzaqui, M.; Semino, R.; Carn, F.; Tavares, S.R.; Menguy, N.; Giménez-Marqués, M.; Bellido, E.; Horcajada, P.; Berthelot, T.; Kuzminova, A.I.; et al. Covalent and Selective Grafting of Polyethylene Glycol Brushes at the Surface of ZIF-8 for the Processing of Membranes for Pervaporation. *ACS Sustain. Chem. Eng.* **2019**, *7*, 6629–6639. [[CrossRef](#)]
14. Georgakilas, V.; Otyepka, M.; Bourlinos, A.B.; Chandra, V.; Kim, N.; Kemp, K.C.; Hobza, P.; Zboril, R.; Kim, K.S. Functionalization of Graphene: Covalent and Non-Covalent Approaches, Derivatives and Applications. *Chem. Rev.* **2012**, *112*, 6156–6214. [[CrossRef](#)]
15. Lashgari, N.; Badiei, A.; Mohammadi Ziarani, G. Modification of mesoporous silica SBA-15 with different organic molecules to gain chemical sensors: A review. *Nanochem. Res.* **2016**, *1*, 127–141. [[CrossRef](#)]
16. Singh, S.; Kumar, R.; Setiabudi, H.D.; Nanda, S.; Vo, D.-V.N. Advanced synthesis strategies of mesoporous SBA-15 supported catalysts for catalytic reforming applications: A state-of-the-art review. *Appl. Catal. A Gen.* **2018**, *559*, 57–74. [[CrossRef](#)]
17. Ndolomingo, M.J.; Meijboom, R. Noble and Base-Metal Nanoparticles Supported on Mesoporous Metal Oxides: Efficient Catalysts for the Selective Hydrogenation of Levulinic Acid to  $\gamma$ -Valerolactone. *Catal. Lett.* **2019**, *149*, 2807–2822. [[CrossRef](#)]

18. Chen, D.; Zhang, P.; Fang, Q.; Wan, S.; Li, H.; Yang, S.; Huang, C.; Dai, S. Coordination-supported organic polymers: Mesoporous inorganic–organic materials with preferred stability. *Inorg. Chem. Front.* **2018**, *5*, 2018–2022. [[CrossRef](#)]
19. Azeez, A.; Polio, L.; Hanson, J.E.; Gorun, S.M. Photoreactive Superhydrophobic Organic–Inorganic Hybrid Materials Composed of Poly(vinylidene fluoride) and Titanium Dioxide-Supported Perfluorinated Phthalocyanines. *ACS Appl. Polym. Mater.* **2019**, *1*, 1514–1523. [[CrossRef](#)]
20. Fedorov, P.P.; Luginina, A.A.; Kuznetsov, S.V.; Voronov, V.V.; Lyapin, A.A.; Ryabochkina, P.A.; Chernov, M.V.; Mayakova, M.N.; Pominova, D.V.; Uvarov, O.V.; et al. Preparation and properties of methylcellulose/nanocellulose/CaF<sub>2</sub>:Ho polymer-inorganic composite films for two-micron radiation visualizers. *J. Fluor. Chem.* **2017**, *202*, 9–18. [[CrossRef](#)]
21. Ahadi, N.; Bodaghifard, M.A.; Mobinikhaledi, A. Cu (II)- $\beta$ -cyclodextrin complex stabilized on magnetic nanoparticles: A retrievable hybrid promoter for green synthesis of spiropyrans. *Appl. Organomet. Chem.* **2019**, *33*, e4738. [[CrossRef](#)]
22. Fallahi, M.; Ahmadi, E.; Mohamadnia, Z. Effect of inorganic oxide supports on the activity of chromium-based catalysts in ethylene trimerization. *Appl. Organomet. Chem.* **2019**, *33*, e4975. [[CrossRef](#)]
23. Li, W.; Zhang, Y.; Li, Q.; Zhang, G. Metal–organic framework composite membranes: Synthesis and separation applications. *Chem. Eng. Sci.* **2015**, *135*, 232–257. [[CrossRef](#)]
24. Yin, P.T.; Shah, S.; Chhowalla, M.; Lee, K.-B. Design, Synthesis, and Characterization of Graphene–Nanoparticle Hybrid Materials for Bioapplications. *Chem. Rev.* **2015**, *115*, 2483–2531. [[CrossRef](#)] [[PubMed](#)]
25. Zhang, N.; Liu, X.; Huang, Y.; Wang, M.; Li, S.; Zong, M.; Liu, P. Novel nanocomposites of cobalt ferrite covalently-grafted on graphene by amide bond as superior electromagnetic wave absorber. *J. Colloid Interface Sci.* **2019**, *540*, 218–227. [[CrossRef](#)]
26. de Sousa, M.E.; Fernández van Raap, M.B.; Rivas, P.C.; Mendoza Zélis, P.; Girardin, P.; Pasquevich, G.A.; Alessandrini, J.L.; Muraca, D.; Sánchez, F.H. Stability and Relaxation Mechanisms of Citric Acid Coated Magnetite Nanoparticles for Magnetic Hyperthermia. *J. Phys. Chem. C* **2013**, *117*, 5436–5445. [[CrossRef](#)]
27. Su, H.; Liu, Y.; Wang, D.; Wu, C.; Xia, C.; Gong, Q.; Song, B.; Ai, H. Amphiphilic starlike dextran wrapped superparamagnetic iron oxide nanoparticle clusters as effective magnetic resonance imaging probes. *Biomaterials* **2013**, *34*, 1193–1203. [[CrossRef](#)]
28. Mrowczynski, R.; Jedrzak, A.; Szutkowski, K.; Grzeskowiak, B.F.; Coy, E.; Markiewicz, R.; Jesionowski, T.; Jurga, S. Cyclodextrin-Based Magnetic Nanoparticles for Cancer Therapy. *Nanomaterials (Basel)* **2018**, *8*. [[CrossRef](#)]
29. Rostamnia, S.; Doustkhah, E. Nanoporous silica-supported organocatalyst: A heterogeneous and green hybrid catalyst for organic transformations. *RSC Adv.* **2014**, *4*, 28238–28248. [[CrossRef](#)]
30. Salvo, A.M.P.; Giacalone, F.; Gruttadauria, M. Advances in Organic and Organic-Inorganic Hybrid Polymeric Supports for Catalytic Applications. *Molecules* **2016**, *21*, 1288. [[CrossRef](#)]
31. Ortuño, M.A.; López, N. Reaction mechanisms at the homogeneous–heterogeneous frontier: Insights from first-principles studies on ligand-decorated metal nanoparticles. *Catal. Sci. Technol.* **2019**, *9*, 5173–5185. [[CrossRef](#)]
32. Karimi, B.; Zamani, A.; Clark, J.H. A Bipyridyl Palladium Complex Covalently Anchored onto Silica as an Effective and Recoverable Interphase Catalyst for the Aerobic Oxidation of Alcohols. *Organometallics* **2005**, *24*, 4695–4698. [[CrossRef](#)]
33. Guo, H.; Gong, C.; Zeng, X.; Xu, H.; Zeng, Q.; Zhang, J.; Zhong, Z.; Xie, J. Isopolymolybdate-based inorganic–organic hybrid compounds constructed by multidentate N-donor ligands: Syntheses, structures and properties. *Dalton Trans.* **2019**, *48*, 5541–5550. [[CrossRef](#)]
34. Goni, M.A.; Rosenberg, E.; Meregude, S.; Abbott, G. A methods study of immobilization of PONOP pincer transition metal complexes on silica polyamine composites (SPC). *J. Organomet. Chem.* **2016**, *807*, 1–10. [[CrossRef](#)]
35. Luca, O.R.; Crabtree, R.H. Redox-active ligands in catalysis. *Chem. Soc. Rev.* **2013**, *42*, 1440–1459. [[CrossRef](#)] [[PubMed](#)]
36. Berben, L.A.; de Bruin, B.; Heyduk, A.F. Non-innocent ligands. *Chem. Commun.* **2015**, *51*, 1553–1554. [[CrossRef](#)]

37. Skorjanc, T.; Benyettou, F.; Olsen, J.C.; Trabolsi, A. Design of Organic Macrocyclic-Modified Iron Oxide Nanoparticles for Drug Delivery. *Chemistry* **2017**, *23*, 8333–8347. [[CrossRef](#)]
38. Velasco, M.I.; Krapacher, C.R.; de Rossi, R.H.; Rossi, L.I. Structure characterization of the non-crystalline complexes of copper salts with native cyclodextrins. *Dalton Trans.* **2016**, *45*, 10696–10707. [[CrossRef](#)]
39. Kurokawa, G.; Sekii, M.; Ishida, T.; Nogami, T. Short Communication: Crystal Structure of a Molecular Complex from Native  $\beta$ -Cyclodextrin and Copper(II) Chloride. *Supramol. Chem.* **2004**, *16*, 381–384. [[CrossRef](#)]
40. Rossi, L.I.; Kinen, C.O.; de Rossi, R.H. Important role of native  $\beta$ -cyclodextrin in the stabilization of transition metal salts. *Comptes Rendus Chim.* **2017**, *20*, 1053–1061. [[CrossRef](#)]
41. Han, B.-H.; Antonietti, M. One-step synthesis of copper nanoparticles containing mesoporous silica by nanocasting of binuclear copper(ii) complexes with cyclodextrins. *J. Mater. Chem.* **2003**, *13*, 1793–1796. [[CrossRef](#)]
42. Bahadorikhali, S.; Ma'mani, L.; Mahdavi, H.; Shafiee, A. Copper supported  $\beta$ -cyclodextrin functionalized PEGylated mesoporous silica nanoparticle-graphene oxide hybrid: An efficient and recyclable nano-catalyst for straightforward synthesis of 2-arylbenzimidazoles and 1,2,3-triazoles. *Microporous Mesoporous Mater.* **2018**, *262*, 207–216. [[CrossRef](#)]
43. Ye, R.-P.; Lin, L.; Liu, C.-Q.; Chen, C.-C.; Yao, Y.-G. One-Pot Synthesis of Cyclodextrin-Doped Cu-SiO<sub>2</sub> Catalysts for Efficient Hydrogenation of Dimethyl Oxalate to Ethylene Glycol. *ChemCatChem* **2017**, *9*, 4587–4597. [[CrossRef](#)]
44. Fedorova, A.A.; Morozov, I.V.; Kotovshchikov, Y.N.; Romanovsky, B.V.; Sirotin, S.V.; Knyazeva, E.E.; Lermontov, A.S.; Shaporev, A.S. Preparation and characterization of copper- and iron-containing mesoporous silica using  $\beta$ -cyclodextrin as a structure-directing agent. *Mendeleev Commun.* **2011**, *21*, 171–172. [[CrossRef](#)]
45. Han, B.-H.; Polarz, S.; Antonietti, M. Cyclodextrin-based Porous Silica Materials as in Situ Chemical “Nanoreactors” for the Preparation of Variable Metal–Silica Hybrids. *Chem. Mater.* **2001**, *13*, 3915–3919. [[CrossRef](#)]
46. Khalafi-Nezhad, A.; Panahi, F. Size-Controlled Synthesis of Palladium Nanoparticles on a Silica–Cyclodextrin Substrate: A Novel Palladium Catalyst System for the Heck Reaction in Water. *ACS Sustain. Chem. Eng.* **2014**, *2*, 1177–1186. [[CrossRef](#)]
47. Martina, K.; Baricco, F.; Caporaso, M.; Berlier, G.; Cravotto, G. Cyclodextrin-Grafted Silica-Supported Pd Nanoparticles: An Efficient and Versatile Catalyst for Ligand-Free C–C Coupling and Hydrogenation. *ChemCatChem* **2016**, *8*, 1176–1184. [[CrossRef](#)]
48. Jayaprabha, K.N.; Joy, P.A. Citrate modified  $\beta$ -cyclodextrin functionalized magnetite nanoparticles: A biocompatible platform for hydrophobic drug delivery. *RSC Adv.* **2015**, *5*, 22117–22125. [[CrossRef](#)]
49. Bagabas, A.A.; Frascioni, M.; Iehl, J.; Hauser, B.; Farha, O.K.; Hupp, J.T.; Hartlieb, K.J.; Botros, Y.Y.; Stoddart, J.F.  $\gamma$ -Cyclodextrin Cuprate Sandwich-Type Complexes. *Inorg. Chem.* **2013**, *52*, 2854–2861. [[CrossRef](#)]
50. Shin, J.-A.; Lim, Y.-G.; Lee, K.-H. Copper-Catalyzed Azide–Alkyne Cycloaddition Reaction in Water Using Cyclodextrin as a Phase Transfer Catalyst. *J. Org. Chem.* **2012**, *77*, 4117–4122. [[CrossRef](#)]
51. Kaboudin, B.; Abedi, Y.; Yokomatsu, T. CuII– $\beta$ -Cyclodextrin Complex as a Nanocatalyst for the Homo- and Cross-Coupling of Arylboronic Acids under Ligand- and Base-Free Conditions in Air: Chemoselective Cross-Coupling of Arylboronic Acids in Water. *Eur. J. Org. Chem.* **2011**, *2011*, 6656–6662. [[CrossRef](#)]
52. Sadeghzadeh, S.M.; Zhiani, R.; Moradi, M. KCC-1 Supported Cu(II)- $\beta$ -Cyclodextrin Complex as a Reusable Catalyst for the Synthesis of 3-Aryl-2-oxazolidinones from Carbon Dioxide, Epoxide, Anilines. *ChemistrySelect* **2018**, *3*, 3516–3522. [[CrossRef](#)]
53. Gupta, D.; Mishra, A.; Kundu, S. Cu (II)- $\beta$ -CD as Water-Loving Catalyst for One-Pot Synthesis of Triazoles and Biofuels Intermediate at Room Temperature without Any Other Additive. *ChemistrySelect* **2017**, *2*, 2997–3008. [[CrossRef](#)]
54. Martina, K.; Calsolaro, F.; Zuliani, A.; Berlier, G.; Chavez-Rivas, F.; Moran, M.J.; Luque, R.; Cravotto, G. Sonochemically-Promoted Preparation of Silica-Anchored Cyclodextrin Derivatives for Efficient Copper Catalysis. *Molecules* **2019**, *24*, 2490. [[CrossRef](#)]
55. Martina, K.; Baricco, F.; Berlier, G.; Caporaso, M.; Cravotto, G. Efficient Green Protocols for Preparation of Highly Functionalized  $\beta$ -Cyclodextrin-Grafted Silica. *ACS Sustain. Chem. Eng.* **2014**, *2*, 2595–2603. [[CrossRef](#)]

56. Musso, G.E.; Bottinelli, E.; Celi, L.; Magnacca, G.; Berlier, G. Influence of surface functionalization on the hydrophilic character of mesoporous silica nanoparticles. *Phys. Chem. Chem. Phys.* **2015**, *17*, 13882–13894. [[CrossRef](#)]
57. Negri, C.; Signorile, M.; Porcaro, N.G.; Borfecchia, E.; Berlier, G.; Janssens, T.V.W.; Bordiga, S. Dynamic Cu-II/Cu-I speciation in Cu-CHA catalysts by in situ Diffuse Reflectance UV-vis-NIR spectroscopy. *Appl. Catal. A Gen.* **2019**, *578*, 1–9. [[CrossRef](#)]
58. Bordiga, S.; Groppo, E.; Agostini, G.; van Bokhoven, J.A.; Lamberti, C. Reactivity of Surface Species in Heterogeneous Catalysts Probed by In Situ X-ray Absorption Techniques. *Chem. Rev.* **2013**, *113*, 1736–1850. [[CrossRef](#)]
59. Solomon, E.I.; Heppner, D.E.; Johnston, E.M.; Ginsbach, J.W.; Cirera, J.; Qayyum, M.; Kieber-Emmons, M.T.; Kjaergaard, C.H.; Hadt, R.G.; Tian, L. Copper Active Sites in Biology. *Chem. Rev.* **2014**, *114*, 3659–3853. [[CrossRef](#)]
60. Negri, C.; Borfecchia, E.; Cutini, M.; Lomachenko, K.A.; Janssens, T.V.W.; Berlier, G.; Bordiga, S. Evidence of Mixed-Ligand Complexes in Cu-CHA by Reaction of Cu Nitrates with NO/NH<sub>3</sub> at Low Temperature. *Chemcatchem* **2019**, *11*, 3828–3838. [[CrossRef](#)]
61. Kau, L.S.; Spirasolomon, D.J.; Pennerhahn, J.E.; Hodgson, K.O.; Solomon, E.I. X-Ray Absorption-Edge Determination of The Oxidation-State and Coordination-Number Of Copper—Application To The Type-3 Site In Rhus-Vernicifera Laccase And Its Reaction With Oxygen. *J. Am. Chem. Soc.* **1987**, *109*, 6433–6442. [[CrossRef](#)]
62. Borfecchia, E.; Beato, P.; Svelle, S.; Olsbye, U.; Lamberti, C.; Bordiga, S. Cu-CHA—A model system for applied selective redox catalysis. *Chem. Soc. Rev.* **2018**, *47*, 8097–8133. [[CrossRef](#)] [[PubMed](#)]
63. Dent, A.J.; Cibir, G.; Ramos, S.; Smith, A.D.; Scott, S.M.; Varandas, L.; Pearson, M.R.; Krumpa, N.A.; Jones, C.P.; Robbins, P.E. B18: A core XAS spectroscopy beamline for Diamond. In Proceedings of the 14th International Conference on X-Ray Absorption Fine Structure, Camerino (MC), Italy, 26–31 July 2009; DiCicco, A., Filipponi, A., Eds.; IOP Publishing: Bristol, UK, 2009; Volume 190.
64. Ravel, B.; Newville, M. Athena, Artemis, Hephaestus: Data analysis for X-ray absorption spectroscopy using IFEFFIT. *J. Synchrotron Radiat.* **2005**, *12*, 537–541. [[CrossRef](#)] [[PubMed](#)]



© 2020 by the authors. Licensee MDPI, Basel, Switzerland. This article is an open access article distributed under the terms and conditions of the Creative Commons Attribution (CC BY) license (<http://creativecommons.org/licenses/by/4.0/>).